Polarized neutron diffraction study of the field-induced magnetization in the normal and superconducting states of $Ba(Fe_{1-x}Co_x)_2As_2$ ($x = 0.65$)

C. Lester,[1] Jiun-Haw Chu,[2,3] J. G. Analytis,[2,3] A. Stunault,[4] I. R. Fisher,[2,3] and S. M. Hayden[1,*]

[1]*H.H. Wills Physics Laboratory, University of Bristol, Tyndall Ave., Bristol, BS8 1TL, United Kingdom*

[2]*Geballe Laboratory for Advanced Materials and Department of Applied Physics, Stanford University, Stanford, California 94305, USA*

[3]*Stanford Institute for Materials and Energy Sciences, SLAC National Accelerator Laboratory, 2575 Sand Hill Road, Menlo Park, California 94025, USA*

[4]*Institut Max von Laue-Paul Langevin, 38042 Grenoble, France*

(Received 21 June 2011; published 13 October 2011)

We use polarized neutron diffraction to study the induced magnetization density of near optimally doped $Ba(Fe_{0.935}Co_{0.065})_2As_2$ ($T_C = 24$ K) as a function of magnetic field ($1 < \mu_0 H < 9$ T) and temperature ($2 < T < 300$ K). The T dependence of the induced moment in the superconducting state is consistent with the Yosida function, characteristic of spin-singlet pairing. The induced moment is proportional to applied field for $\mu_0 H \leqslant 9\,\mathrm{T} \approx \mu_0 H_{c2}/6$. In addition to the Yosida spin-susceptibility, our results reveal a large zero-field contribution $M(H \to 0, T \to 0)/H \approx 2/3\chi_{\mathrm{normal}}$ which does not scale with the field or number of vortices and is most likely due to the van Vleck susceptibility. Magnetic structure factors derived from the polarization dependence of 15 Bragg reflections were used to make a maximum entropy reconstruction of the induced magnetization distribution in real space. The magnetization is confined to the Fe atoms, and the measured density distribution is in good agreement with LAPW band structure calculations which suggest that the relevant bands near the Fermi energy are of the $d_{xz/yz}$ and d_{xy} type.

DOI: 10.1103/PhysRevB.84.134514 PACS number(s): 74.70.Xa, 74.25.Jb, 74.25.N−, 75.25.−j

I. INTRODUCTION

The discovery of superconductivity in iron-based materials such as $LaO_{1-x}F_xFeAs$[1] has ignited intense interest in this field. The common features of the iron-based superconductors appear to be that they are semi-metals which have electron and hole Fermi surface pockets, separated by a (π,π) wave vector.[2] Experiments have demonstrated the existence of strong spin excitations with this same wave vector for superconducting compositions. It is widely believed that iron-based superconductivity is mediated by these spin excitations resulting in superconducting states such as $s_{\pm}$, where the sign of the gap changes between different Fermi surface sheets.

Of particular interest in the iron-based superconductors is the structure of the superconducting gap and the nature of the low-energy electronic states. Penetration depth[3] and thermal conductivity studies[4] of a number of materials [e.g., LaFePO, KFe_2As_2, and $BaFe_2(As_{1-x}P_x)_2$] show evidence for low-energy quasiparticle excitations which could be due to nodes in the superconducting order parameter.

$Ba(Fe_{1-x}Co_x)_2As_2$ is a good system to study since it is possible to grow large single crystals with homogeneous doping. It has been widely studied by various probes including angle-resolved photoemission spectroscopy (ARPES),[5] scanning tunnel microscopy (STM),[6] penetration depth,[7,8] μSR,[9] heat capacity,[10,11] and thermal conductivity.[4] Even in this single system, different gap characters have been proposed as a function of doping, including fully and nodally gapped structures.[4–7,9–11]

Here we use half-polarized neutron diffraction to measure the susceptibility and induced magnetization in the normal and superconducting states of near optically doped $Ba(Fe_{1-x}Co_x)_2As_2$ ($x = 0.065$). Our measurements shed light on the electronic structure and the nature of the low-energy electronic states in both phases. By measuring the flipping ratios of a number of Bragg peaks, we are able to extract the spatial Fourier components of the induced magnetization density $\mathbf{M}(\mathbf{r})$. In a metal, this provides information about the electronic states near the Fermi energy. We compare our results with a band structure calculation. In addition to measuring the $\mathbf{M}(\mathbf{r})$, we also made a detailed study of the temperature and magnetic field dependence of the induced magnetization by measuring a single Bragg peak in detail.

The paper is organized as follows. In Sec. II, we introduce the polarized beam method used in our experiment and report our unpolarized structural refinement of $Ba(Fe_{1-x}Co_x)_2As_2$ ($x = 0.065$). In Sec. III, we report our determination of the real space magnetization density $\mathbf{M}(\mathbf{r})$ induced by an applied magnetic field. We also present the results of a LAPW calculation of the magnetization density distribution. In Sec. IV, we report measurements of the induced magnetization *in the superconducting state* as a function of magnetic field and temperature. We discuss the significance of our observations with respect to the superconductivity in $Ba(Fe_{1-x}Co_x)_2As_2$ ($x = 0.065$) and other experimental results. This is followed by a summary of our conclusions.

II. BACKGROUND

A. Polarized Neutron Diffraction Studies of the Induced Magnetization

Polarized neutron scattering experiments can directly measure the real-space magnetization density $\mathbf{M}(\mathbf{r})$ in the unit cell, induced by a large magnetic field $\mu_0 H$. Due to the periodic crystal structure, the applied magnetic field induces a

magnetization density with spatial Fourier components $\mathbf{M}(\mathbf{G})$, where $\mathbf{G}$ are the reciprocal lattice vectors, such that

$$\mathbf{M}(\mathbf{r}) = \frac{1}{v_0}\sum_{\mathbf{G}} \mathbf{M}(\mathbf{G}) \exp(-i\mathbf{G}\cdot\mathbf{r}) \quad (1)$$

and v_0 is the volume of the unit cell. The Fourier components of the magnetization density are given by

$$\mathbf{M}(\mathbf{G}) = \int_{\text{unit cell}} \mathbf{M}(\mathbf{r}) \exp(i\mathbf{G}\cdot\mathbf{r}) d\mathbf{r}. \quad (2)$$

Neutrons interact with matter through the strong nuclear force and electromagnetic interaction. For neutrons with initial and final spin polarizations σ_i and σ_f, the total scattering cross section is

$$\left(\frac{d\sigma}{d\Omega}\right)_{\sigma_i\to\sigma_f} \propto \left|\langle\sigma_i|\frac{\gamma r_0}{2\mu_B}\boldsymbol{\sigma}\cdot\hat{\mathbf{G}}\times\{\mathbf{M}(\mathbf{G})\times\hat{\mathbf{G}}\} + F_N(\mathbf{G})|\sigma_f\rangle\right|^2, \quad (3)$$

where $\gamma r_0 = 5.36\times10^{-15}$ m and $F_N(\mathbf{G})$ is the nuclear structure factor. The sign of the first (magnetic) term in Eq. (3) can be changed by reversing the incident neutron polarization. Thus we are able to isolate the interference term between the nuclear and magnetic scattering. In this experiment, we measure the flipping ratio R, defined as the ratio of the crosssections with neutrons parallel and antiparallel to the applied magnetic field. Because the induced moment is small, the experiment is carried out in the limit $(\gamma r_0/2\mu_B)M(\mathbf{G})/F_N(\mathbf{G}) \ll 1$. In this limit, the flipping ratio derived from Eq. (3) is,

$$R = \frac{|F_N(\mathbf{G}) - (\gamma r_0/2\mu_B)M(\mathbf{G})|^2}{|F_N(\mathbf{G}) + (\gamma r_0/2\mu_B)M(\mathbf{G})|^2} \approx 1 - \frac{2\gamma r_0}{\mu_B}\frac{M(\mathbf{G})}{F_N(\mathbf{G})}. \quad (4)$$

As the nuclear structure factors $F_N(\mathbf{G})$ are known from the crystal structure, Eq. (4) directly gives $M(\mathbf{G})$.

B. Experimental Details

The $Ba(Fe_{1-x}Co_x)_2As_2$ ($x = 0.065$) single crystal used in this study was prepared by a self-flux method,[12] had approximate dimensions $6\times1.5\times0.2$ mm^3, and a mass of $\sim$1.8 mg. Similar samples were used in our previous studies.[13,14] Resistivity and magnetization measurements on crystals from the same batch identified the superconducting transition temperature T_c(onset) = 24 K and showed no evidence of magnetic order down to 2 K. The bulk susceptibility in a 5 T field measured using a SQUID magnetometer was $\chi_{ab} = 1.22\times10^{-3}\ \mu_B\ \text{T}^{-1}\,\text{f.u.}^{-1}$. We note that the expected upper critical field applied in the ab plane for this composition is $H_{c2,ab} = 55$ T.[15]

Neutron scattering experiments were performed at the Institut Laue-Langevin, Grenoble, France. An initial unpolarized structural refinement was performed using the 4-circle D9 spectrometer with $\lambda = 0.837(1)$ Å. The results are shown in Table I. Polarized beam measurements of the flipping ratio were made on the D3 spectrometer. The sample was mounted on a thin aluminium post with the $[1\bar{1}0]$ direction vertical and parallel to the applied field. Data was collected with an incident wavelength $\lambda = 0.825$ Å and a 0.5 mm Er filter (to reduce higher order contamination in the incident beam). Flipping ratios for equivalent reflections were collected, averaged, and corrected for the finite beam polarization and extinction effects. The sample was cooled through T_c at each field measured when collecting data in the superconducting state.

TABLE I. Structural parameters of $Ba(Fe_{1-x}Co_x)_2As_2$ ($x = 0.065$). Parameters are obtained from least-squares refinement of integrated intensities measured at $T = 30$ K on D9. The B factor is related to the mean squared atomic displacement $\langle u^2\rangle$ by $B = 8\pi^2\langle u^2\rangle$. g is the width parameter of the mosaic distribution (Refs. 16 and 17).

Atom	Position in I4/mmm		z	B (Å^2)
Ba	2a	(0 0 0)		0.020(16)
Fe/Co	4d	$\left(\frac{1}{2}\ 0\ \frac{1}{4}\right)$		0.110(10)
As	4e	(0 0 z)	0.3534(1)	0.080(11)
$a = 3.952(2)$ Å, $c = 12.911(15)$ Å				
$g = 22.4(1.2)$ rad^{-1}				

III. INDUCED MAGNETIZATION DISTRIBUTION

A. Results

We measured the magnetization induced by a 9 T magnetic field applied along the $[1\bar{1}0]$ direction in the normal state at $T = 30$ K. Table II shows the measured flipping ratios under these conditions and the extracted Fourier components of the magnetization density. Figure 1 shows $|M(\mathbf{G})|$ plotted against $\sin\theta/\lambda = |\mathbf{G}|/4\pi$. If Fe were the only magnetic atom, then the sign of $M(\mathbf{G})$ is determined by the geometric structure factor for the Fe atoms and $|M(\mathbf{G})|$ is the effective form factor of the Fe atom. The solid line in Fig. 1 is the standard calculated isotropic atomic form factor for Fe^{2+}.[19] Deviations

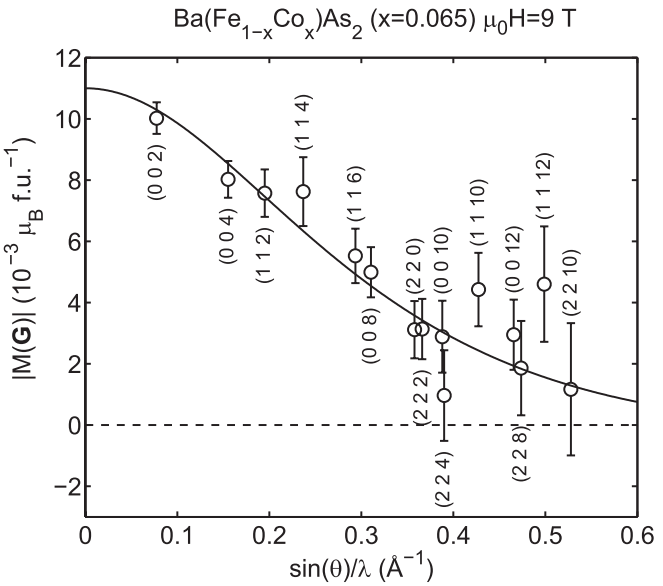

FIG. 1. The magnetic structure factors $|M(\mathbf{G})|$ measured for a 9 T field applied along the $[1\bar{1}0]$ direction. The solid line is the Fe^{2+} form factor[19] scaled to the measured susceptibility.

TABLE II. For each Bragg reflection (hkl), the table shows: $\sin\theta/\lambda$, the measured flipping ratio R, structure factor $F_N(\mathbf{G})$ calculated from the structure in Table I, and the determined magnetic structure factor $M(\mathbf{G})$.[18] Data collected at $T = 30$ K and $\mu_0 H = 9$ T.

h	k	l	$\sin\theta/\lambda$ (Å^{-1})	$(1-R)\times10^3$	$F_N(\mathbf{G})$ (fm f.u.$^{-1}$)	$M(\mathbf{G})$ (mμ_B f.u.$^{-1}$)
2	2	0	0.3611	0.83 ± 0.3	36.16	3.1 ± 0.9
0	0	2	0.0780	4.98 ± 0.3	-16.88	-10.0 ± 0.5
1	1	2	0.1967	3.75 ± 0.5	19.93	7.5 ± 0.8
2	2	2	0.3694	1.90 ± 0.6	-16.54	-3.1 ± 1.0
0	0	4	0.1560	6.49 ± 0.5	12.19	8.0 ± 0.6
1	1	4	0.2386	3.08 ± 0.5	-24.46	-7.6 ± 1.1
2	2	4	0.3933	0.8 ± 1.3	12.04	0.9 ± 1.5
1	1	6	0.2956	1.61 ± 0.2	32.68	5.5 ± 0.9
0	0	8	0.3120	1.58 ± 0.4	29.32	4.9 ± 0.8
2	2	8	0.4772	1.18 ± 0.7	28.90	1.8 ± 1.5
0	0	10	0.3900	1.12 ± 0.5	-25.57	-2.8 ± 1.2
1	1	10	0.4298	4.52 ± 1.2	10.42	4.4 ± 1.2
2	2	10	0.5315	3.60 ± 2.9	-25.11	-1.1 ± 2.2
0	0	12	0.4681	0.72 ± 0.6	23.42	2.9 ± 1.2
1	1	12	0.5017	3.29 ± 4.5	-12.16	-4.6 ± 1.9

from an isotropic form factor are expected at larger θ or $|\mathbf{G}|$. Our results are in broad agreement with a recent study of $Ba(Fe_{1-x}Co_x)_2As_2$ ($x = 0.066$).[20] The main differences between the present data and the data presented in Ref. 20 are: (i) the present study has higher statistical accuracy, (ii) the value of $M(\mathbf{G})$ for $\mathbf{G} = (002)$ is larger relative to the other $\mathbf{G}$ points in the present study. Our extinction model shows that the (002) peak has the largest extinction correction factor of 1.26.

We used the maximum entropy method (MaxEnt)[21–24] to make a model-free reconstruction of the magnetization density in real space. Flipping ratios for reflections of the type (hhl) were collected; this allowed the reconstruction of the magnetization density projected down the $[1\bar{1}0]$ direction onto the (110) plane as illustrated in the left panel of Fig. 2. The result of the reconstruction is shown in the right panel of Fig. 2. As expected, the magnetization density is localized mostly on the Fe atoms. The magnetization "cloud" appears to be slightly extended along the ⟨110⟩ directions. Our results are in broad agreement with Ref. 20, however we observe no significant magnetization density on the Ba sites. A recent study of the paramagnetic state of the parent antiferromagnet $BaFe_2As_2$[24] is also broadly consistent with our results. The main difference in the $BaFe_2As_2$ case is that the magnetization extends more toward the As atoms.

B. Electronic Structure Calculations

Induced form factor measurements have been widely used to determine the nature of the electrons responsible for paramagnetism in solids. In metals, the induced magnetization arises from a redistribution of electrons between up and down states near the Fermi energy. Thus, we probe the nature of the electronic wave functions for states near the Fermi energy. In order to understand our results further, we have carried out electronic structure calculations using the WEIN2K package.[25] Our calculations complement magnetic form factor calculations of the antiferromagnetic parent compound $SrFe_2As_2$.[26]

The linear augmented plane-wave (LAPW) method[27] was used to obtain the electronic structure and spin density of $Ba(Fe_{1-x}Co_x)_2As_2$ ($x = 0.065$). We used a full-potential LAPW method with the generalized gradient approximation (GGA). In the case of doped compositions, we used the virtual

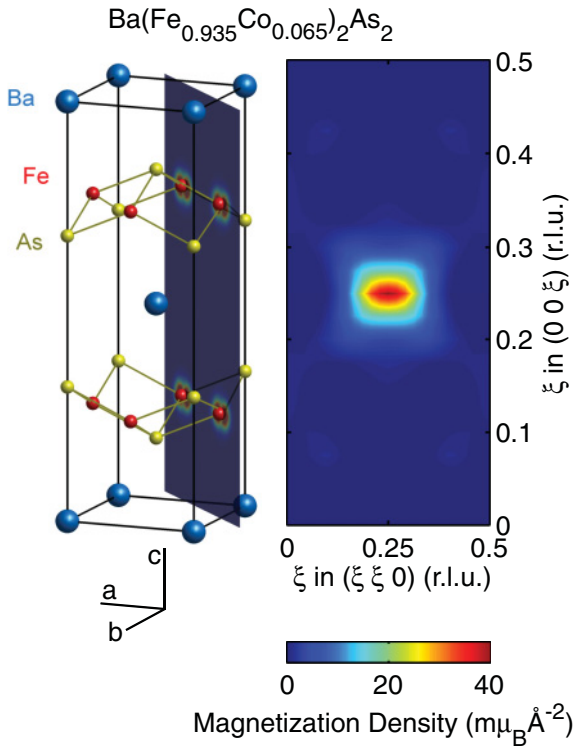

FIG. 2. (Color online) (left) The conventional tetragonal unit cell of $Ba(Fe,Co)_2As_2$. We measure the magnetization density integrated perpendicular to the (110)-type plane shown. The magnetization density shown is the result of the VCA calculation shown in Fig. 4. (right) Projected magnetization distribution reconstructed from the experimental data in Table. II. The reconstructed magnetization map shows $\frac{1}{4}$ of the area of the plane shown in the left panel.

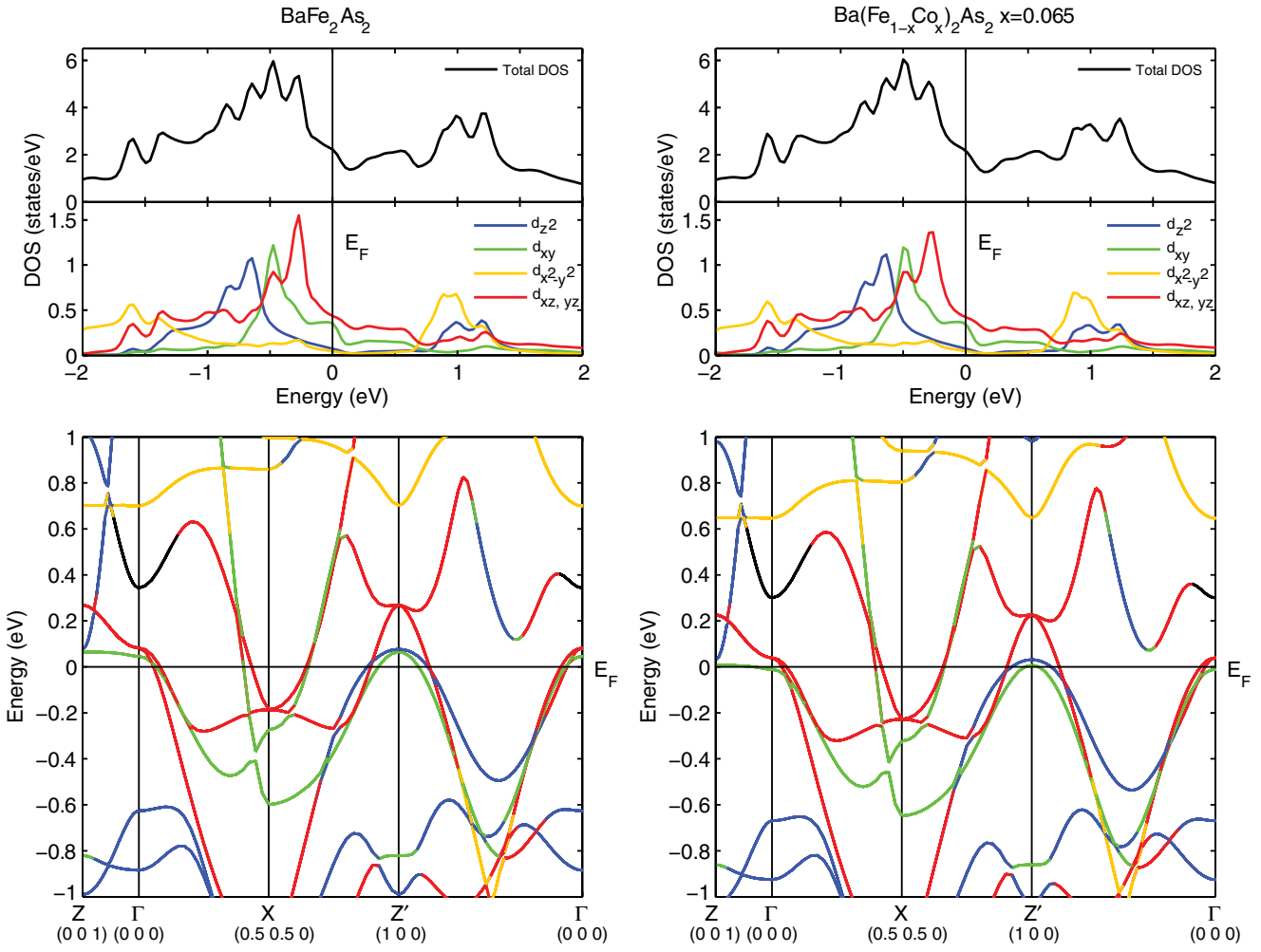

FIG. 3. (Color online) (bottom panels) The LAPW band-structure calculations for $Ba(Fe_{1-x}Co_x)_2As_2$ for $x = 0$ (left) and $x = 0.065$ (right) in the VCA. Colors indicate the dominant orbital of the **k** state. (top panels) Calculated electronic density of states.

crystal approximation (VCA).[28] We used the lattice parameters and atom positions for the $Ba(Fe_{1-x}Co_x)_2As_2$ ($x = 0.065$) structure shown in Table. II for both compositions. The muffin-tin radii were chosen to be 2.5, 2.37, and 2.11 atomic units (a.u.) for Ba, Fe, and As, respectively, with the quantity $R_{MT}K_{max}$ set to 7, where R_{MT} is the smallest muffin-tin radius and K_{max} is the plane wave cutoff. For integrations we used 726 k points in the irreducible Brillouin zone. In the LAPW method, the charge (spin) density is represented by a plane wave expansion in the interstitial region and as a combination of radial functions times spherical harmonics inside the muffin-tin spheres. Figure 3 shows the band structure calculated in the tetragonal phase for $Ba(Fe_{1-x}Co_x)_2As_2$ for $x = 0$ and $x = 0.065$. Our calculations generally agree with others in the literature;[29–32] in particular, they show that the states near the Fermi energy are predominately of $d_{xz,yz}$ and d_{xy} character.

Spin polarized calculations were carried out in the tetragonal state with the ferromagnetic magnetization constrained to be 0.01 μ_B per unit cell to mimic the effect of an applied magnetic field. The results were then scaled to the measured magnetization at $\mu_0 H = 9$ T for comparison purposes. The results are shown in Fig. 4. The $x = 0.065$ calculation shows reasonable agreement with our maximum entropy reconstruction in that the magnetization density is extended along the $\langle 110 \rangle$ direction. However, the reconstruction from our experimental data does not show the two maxima along $(\xi,\xi,1/2)$ predicted in the calculation. This is presumably because our data have insufficient Fourier components to resolve these features. We also carried out a calculation for $BaFe_2As_2$ ($x = 0$) in the paramagnetic tetragonal state with the same structural parameters (but no Co potential) to demonstrate the sensitivity of the magnetization distribution to the band structure. Notice that the change in electronic structure between $x = 0$ and $x = 0.065$ causes a rotation of the calculated pattern in Fig. 4.

IV. TEMPERATURE AND FIELD DEPENDENCE OF THE MAGNETIZATION

The measurement of the field and temperature dependence of bulk magnetization $M(H,T)$ in the mixed state of a superconductor provides information about the nature of the superconductive pairing. Thermal conductivity $\kappa(H,T,\theta)$[4] and specific heat measurements $C = \gamma(H)T$[33] in the mixed state have been extremely useful in probing the low-energy quasi

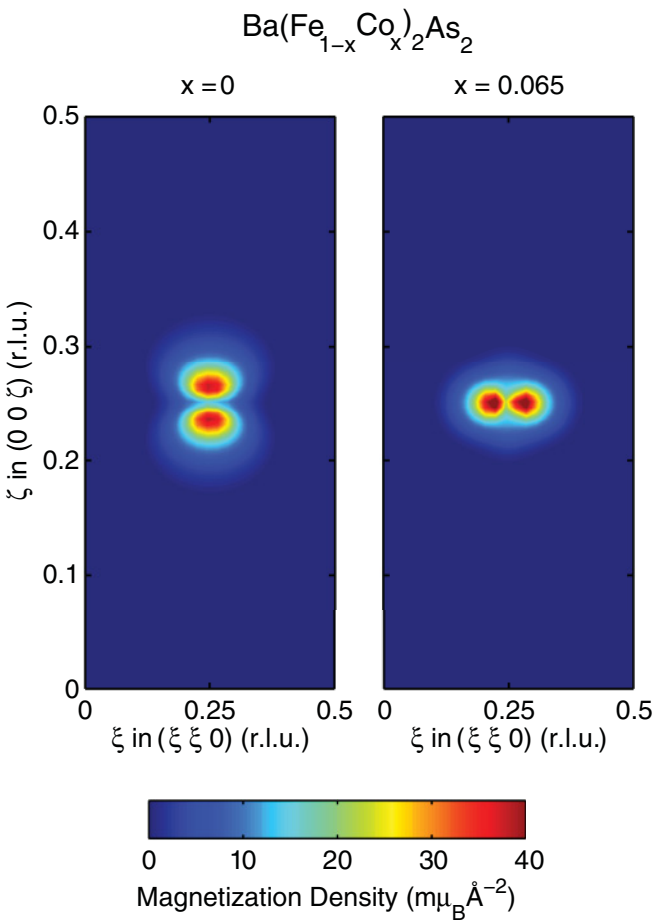

FIG. 4. (Color online) Magnetization density of $Ba(Fe_{1-x}Co_x)_2As_2$ calculated using the LAPW method and VCA approximation for $x = 0$ (left panel) and $x = 0.065$ (right panel). Calculations were carried out with a small fixed ferromagnetic moment to mimic the effect of an applied field.

particles and identified the gap structure of a number of superconductors. In particular, the field dependence of the electronic contributions to κ and C in the $T \to 0$ limit is sensitive to the symmetry of the superconducting gap function[34] (see Fig. 5). Complementary information is contained in $M(H,T)$. However, studies of the bulk magnetization in the mixed state of superconductors are not possible by conventional means, e.g., SQUID magnetometery, because of the presence of a large diamagnetic contribution. Polarized neutron diffraction and NMR Knight shift measurements[36,37] can be used to make magnetization measurements in the mixed state. The polarized neutron diffraction technique used here is unique because it directly measures the total magnetization including spin and orbital contributions. This technique was first used by Shull and Wedgwood in 1963 to study V_3Si,[38] and has subsequently been applied to such varied superconductors as UPt_3,[39] $YBa_2Cu_3O_{7-\delta}$,[40] and Sr_2RuO_4.[41]

A. Results

We used the (002) Bragg peak to make our measurement since this requires little correction to give the $\mathbf{G} = 0$ magnetization, $M[\mathbf{G} = (002)]/M(\mathbf{G} = 0) = 0.979$ for an isotropic

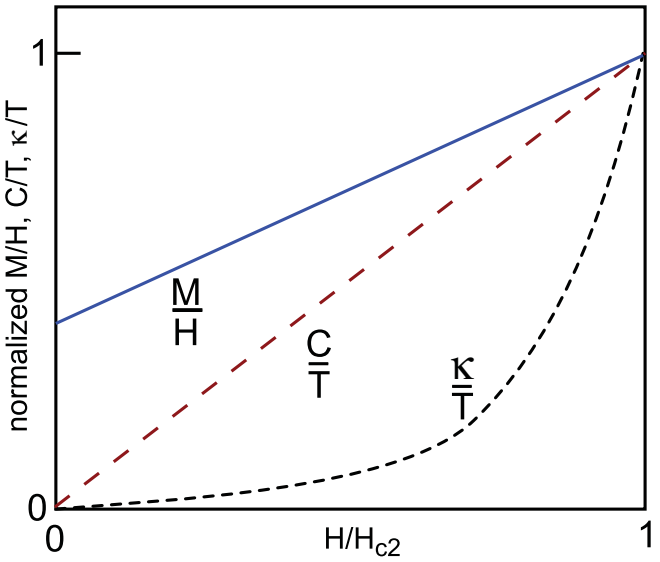

FIG. 5. (Color online) Schematic field dependence of the low-temperature magnetization M, specific heat C, and thermal conductivity κ for an s-wave superconductor. The behavior for C and κ are based on V_3Si.[35]

Fe^{2+} ion. Figure 6 shows the temperature dependence of the induced magnetization of $Ba(Fe_{1-x}Co_x)_2As_2$ ($x = 0.065$) for $\mu_0 H = 9$ T. The temperature dependence shows the characteristic Yosida dependence expected for singlet pairing;[42] this is consistent with measurements of the NMR Knight shift in the same compound.[36,37] There is a large susceptibility in the $T \to 0$ limit. A large residual contribution is also observed in V_3Si,[38] and this has been attributed to the van Vleck contribution.[43] The presence of large van Vleck contribution has also been inferred[44,45] from NMR knight shift measurements on other iron-based superconductors. Figure 7 (top panel) shows the field dependence of the induced magnetization. $M(\mathbf{G}) \propto H$ over the field range of the present experiment ($\mu_0 H < 9$ T). When we plot the susceptibility $M(\mathbf{G})/H$ [see Fig. 7 (bottom panel)], we find that the value as $T \to 0$ and $H \to 0$ is about $\frac{2}{3}$ of the normal state value measured at T_c in the present experiment.

B. Interpretation

We measured the static response at finite wave vector $\mathbf{G}$ to an (approximately) uniform magnetic field, that is, $\chi(\mathbf{G}) \equiv \chi(\mathbf{G},0) = M(\mathbf{G})/H(\mathbf{G} = 0)$.[18,46] The atomic nature of solids means that the induced magnetization $M(\mathbf{r})$ is spatially modulated on an atomic scale (see Fig. 2). Neutrons diffract from this modulation. In the mixed state of a superconductor, there is an additional diamagnetic magnetization (which gives rise to the vortex lattice), which is not detected in the present experiment. The signal from the vortex lattice is only present at small wave vectors (scattering angles) and can be studied by neutrons using small angle scattering techniques. In the following discussion, we do not include the superconducting diamagnetic response.

The magnetic susceptibility in d-band metals has several components: atomic diamagnetic, van Vleck ("orbital" or "interband"), and spin. The atomic diamagnetic contribution

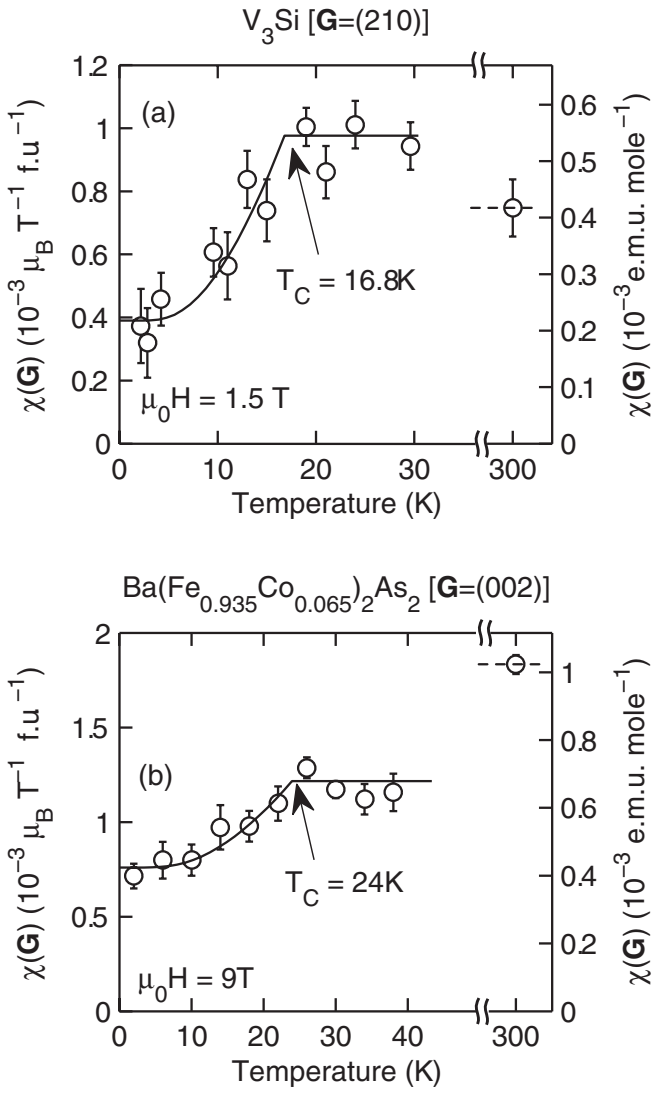

FIG. 6. The temperature dependence of the susceptibility and induced moment of V_3Si[38] (top panel) and $Ba(Fe_{1-x}Co_x)_2As_2$ $x = 0.065$ (bottom panel) measured using polarized neutron scattering. The solid lines are the Yosida behavior expected for a singlet order parameter.

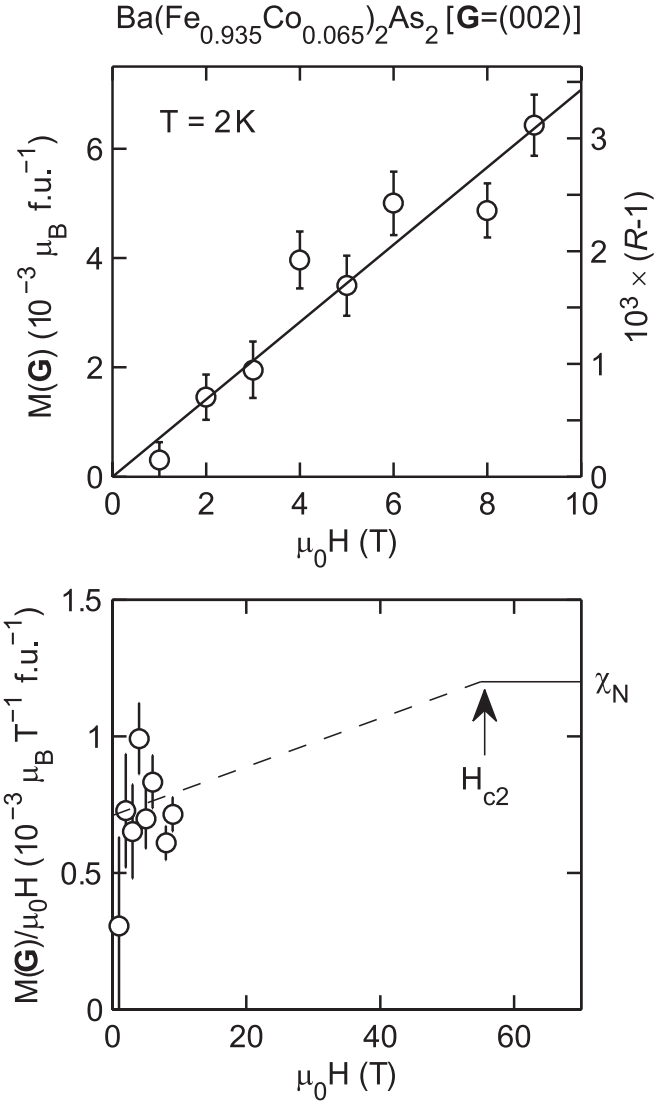

FIG. 7. (Top panel) Field dependence of the induced magnetization $M(\mathbf{G})$ of $Ba(Fe_{1-x}Co_x)_2As_2$ $x = 0.065$ measured at $T = 2$ K. R is the corresponding flipping ratio. (Bottom panel) $M(\mathbf{G})/H$. The dashed line corresponds to the approximation $M_{\rm spin} \propto H^2$.

in $BaFe_2As_2$ has been estimated[24] to be small and is neglected here. Only the spin contribution is expected to be suppressed by singlet Cooper pairing, thus we write the spatially averaged induced magnetization in the mixed state as

$$M = \chi_{\rm orb} H + M_{\rm spin}(T, H), \tag{5}$$

where $\chi_{\rm orb}$ is the orbital susceptibility and $M_{\rm spin}$ is the spin magnetization. In an s-wave superconductor, the density of states due to the introduction of vortices is $\propto N_F H/H_{c2}$.[47,48] Thus the spin magnetization should vary as $M_{\rm spin}(T \to 0, H) \propto H^2$. The temperature dependence is given by the Yosida function,[42] $M_{\rm spin}(T, H \to 0) \propto Y(T)$. The present experiments (Fig. 7) show that the differential susceptibility dM/dH has a large finite value in the $H \to 0$ limit and $dM/dH \approx$ constant for $\mu_0 H < 9$ T. This is consistent with the finite $\chi(T \to 0, H \to 0)$ response being due to a van Vleck contribution. It should be noted that there is also NMR evidence for a residual susceptibility in $BaFe_2(As_{0.67}P_{0.33})_2$[49] and $Ba(Fe_{0.93}Co_{0.07})_2As_2$.[37] Specific heat measurements also suggest that there can be a sizable residual quasiparticle density of states in $Ba(Fe_{1-x}Co_x)_2As_2$.[10,11,50] We cannot rule out the possibility that this is related to the residual susceptibility observed by neutron scattering.

There has been considerable debate about the nature of the superconducting gap in $Ba(Fe_{1-x}Co_x)_2As_2$. In principle, a detailed measurement of the T dependence of the induced moment could be used to distinguish between different models for the gap. Unfortunately, the statistical noise in the present data is relatively high. Thus we make only a basic comparison with a singlet s-wave state. Within the statistical error of our data, the temperature dependent component of the induced moment $M_{\rm spin}$ is well described by a Yosida temperature dependence (see Fig. 6) with $\Delta = 1.78 k_B T = 41$ K $= 3.5$ meV.

V. CONCLUSIONS

We have used a polarized neutron diffraction technique to measure the induced magnetization density of near optimally doped $Ba(Fe_{0.935}Co_{0.065})_2As_2$ ($T_C = 24$ K) as a function of magnetic field and temperature. The induced magnetization is confined to the Fe atoms with an oblate distribution spread out in the ab plane. The distribution is in reasonable agreement with a full potential LAPW band structure calculation which suggests that the relevant bands near the Fermi energy are of the $d_{xz/yz}$ and d_{xy} type.

The T dependence of the induced moment in the superconducting state is consistent with the Yosida function characteristic of spin-singlet pairing, and the induced moment is proportional to applied field for $\mu_0 H \leqslant 9\text{T} \approx \mu_0 H_{c2}/6$. We observe a large residual susceptibility $M(H \to 0, T \to 0)/H \approx 2/3\chi_{\text{normal}}$. This is most easily interpreted as being due to the van Vleck contribution present in other d-band systems, but may also signal a residual quasiparticle density of states.

ACKNOWLEDGMENTS

We thank P. J. Brown, A. Carrington, P. J. Hirschfeld and I. I. Mazin for helpful discussions. Work at Stanford was supported by the Department of Energy, Office of Basic Energy Sciences under Contract No. DE-AC02-76SF00515.

*s.hayden@bris.ac.uk

[1] Y. Kamihara, T. Watanabe, M. Hirano, and H. Hosono, J. Am. Chem. Soc. **130**, 3296 (2008).

[2] A new class of materials AFe_xSe_2 (A = K, Rb, Cs, Tl) (Ref. 51) has recently been discovered. How these fit into the general picture remains to be seen (Ref. 52).

[3] J. D. Fletcher, A. Serafin, L. Malone, J. G. Analytis, J.-H. Chu, A. S. Erickson, I. R. Fisher, and A. Carrington, Phys. Rev. Lett. **102**, 147001 (2009).

[4] J.-P. Reid, M. A. Tanatar, X. G. Luo, H. Shakeripour, N. Doiron-Leyraud, N. Ni, S. L. Bud'ko, P. C. Canfield, R. Prozorov, and L. Taillefer, Phys. Rev. B **82**, 064501 (2010).

[5] K. Terashima, Y. Sekiba, J. H. Bowen, K. Nakayama, T. Kawahara, T. Sato, P. Richard, Y.-M. Xu, L. J. Li, G. H. Cao, Z.-A. Xu, H. Ding, and T. Takahashi, PNAS **106**, 7330 (2009).

[6] Y. Yin, M. Zech, T. L. Williams, X. F. Wang, G. Wu, X. H. Chen, and J. E. Hoffman, Phys. Rev. Lett. **102**, 097002 (2009).

[7] R. T. Gordon, H. Kim, N. Salovich, R. W. Giannetta, R. M. Fernandes, V. G. Kogan, T. Prozorov, S. L. Bud'ko, P. C. Canfield, M. A. Tanatar, and R. Prozorov, Phys. Rev. B **82**, 054507 (2010).

[8] L. Luan, T. M. Lippman, C. W. Hicks, J. A. Bert, O. M. Auslaender, J.-H. Chu, J. G. Analytis, I. R. Fisher, and K. A. Moler, Phys. Rev. Lett. **106**, 067001 (2011).

[9] T. J. Williams, A. A. Aczel, E. Baggio-Saitovitch, S. L. Bud'ko, P. C. Canfield, J. P. Carlo, T. Goko, J. Munevar, N. Ni, Y. J. Uemura, W. Yu, and G. M. Luke, Phys. Rev. B **80**, 094501 (2009).

[10] M. Gang, Z. Bin, C. Peng, W. Zhao-Sheng, F. Lei, S. Bing, S. Lei, R. Cong, and W. Hai-Hu, Chin. Phys. Lett. **27**, 037402 (2010).

[11] K. Gofryk, A. B. Vorontsov, I. Vekhter, A. S. Sefat, T. Imai, E. D. Bauer, J. D. Thompson, and F. Ronning, Phys. Rev. B **83**, 064513 (2011).

[12] J.-H. Chu, J. G. Analytis, C. Kucharczyk, and I. R. Fisher, Phys. Rev. B **79**, 014506 (2009).

[13] C. Lester, J.-H. Chu, J. G. Analytis, S. C. Capelli, A. S. Erickson, C. L. Condron, M. F. Toney, I. R. Fisher, and S. M. Hayden, Phys. Rev. B **79**, 144523 (2009).

[14] C. Lester, J.-H. Chu, J. G. Analytis, T. G. Perring, I. R. Fisher, and S. M. Hayden, Phys. Rev. B **81**, 064505 (2010).

[15] M. Kano, Y. Kohama, D. Graf, F. Balakirev, A. S. Sefat, M. A. Mcguire, B. C. Sales, D. Mandrus, and S. W. Tozer, J. Phys. Soc. Jpn. **78**, 084719 (2009).

[16] P. J. Becker and P. Coppens, Acta Cryst. A **30**, 129 (1974).

[17] The extinction calculation assumed a Lozentzian mosaic distribution with a domain radius $r = 300$ nm.

[18] The signs (phases) of $F_N(\mathbf{G})$ and $M(\mathbf{G})$ depend of the origin chosen for the unit cell in Eq. (2). The values in Table I are used here.

[19] P. J. Brown, *International Tables for Crystallography* (Kluwer, Dordrecht, 1992), p. 391.

[20] K. Prokes, A. Gukasov, D. N. Argyriou, S. L. Bud'ko, P. C. Canfield, A. Kreyssig, and A. I. Goldman, Europhys. Lett. **93**, 32001 (2011).

[21] *Maximum Entropy and Bayesian Methods*, edited by J. Skilling (Kluwer, Dordrecht, 1989).

[22] R. J. Papoular and B. Gillon, Europhys. Lett. **13**, 429 (1990).

[23] S. F. Gull and J. Skilling, *MEMSYS III Quantified Maximum Entropy Subroutine Library* (Meldreth, UK, 1989).

[24] P. J. Brown, T. Chatterji, A. Stunault, Y. Su, Y. Xiao, R. Mittal, T. Brückel, T. Wolf, and P. Adelmann, Phys. Rev. B **82**, 024421 (2010).

[25] P. Blaha, K. Schwarz, G. K. H. Madsen, D. Kvasnicka, and J. Luitz, *WIEN2k, An Augmented Plane Wave + Local Orbitals Program for Calculating Crystal Properties* (Karlheinz Schwarz, Techn. Universität Wien, Austria, 2001).

[26] Y. Lee, D. Vaknin, H. Li, W. Tian, J. L. Zarestky, N. Ni, S. L. Bud'ko, P. C. Canfield, R. J. McQueeney, and B. N. Harmon, Phys. Rev. B **81**, 060406 (2010).

[27] David J. Singh and Lars Nordström, *Planewaves, Pseudopotentials and the LAPW Method* (Springer, New York, 2006).

[28] L. Nordheim, Ann. Phys. **401**, 607 (1931).

[29] D. J. Singh, Phys. Rev. B **78**, 094511 (2008).

[30] S. Thirupathaiah, S. de Jong, R. Ovsyannikov, H. A. Dürr, A. Varykhalov, R. Follath, Y. Huang, R. Huisman, M. S. Golden, Y.-Z. Zhang, H. O. Jeschke, R. Valentí, A. Erb, A. Gloskovskii, and J. Fink, Phys. Rev. B **81**, 104512 (2010).

[31] O. Andersen and L. Boeri, Ann. Phys. **523**, 8 (2011).

[32] N. Colonna, G. Profeta, A. Continenza, and S. Massidda, Phys. Rev. B **83**, 094529 (2011).

[33] K. A. Moler, D. L. Sisson, J. S. Urbach, M. R. Beasley, A. Kapitulnik, D. J. Baar, R. Liang, and W. N. Hardy, Phys. Rev. B **55**, 3954 (1997).

[34] H. Shakeripour, C. Petrovic, and L. Taillefer, New J. Phys. **11**, 055065 (2009).

[35]E. Boaknin, M. A. Tanatar, J. Paglione, D. Hawthorn, F. Ronning, R. W. Hill, M. Sutherland, L. Taillefer, J. Sonier, S. M. Hayden, and J. W. Brill, Phys. Rev. Lett. **90**, 117003 (2003).

[36]F. Ning, K. Ahilan, T. Imai, A. S. Sefat, R. Jin, M. A. McGuire, B. C. Sales, and D. Mandrus, J. Phys. Soc. Jpn. **77**, 103705 (2008).

[37]S. Oh, A. M. Mounce, S. Mukhopadhyay, W. P. Halperin, A. B. Vorontsov, S. L. Bud'ko, P. C. Canfield, Y. Furukawa, A. P. Reyes, and P. L. Kuhns, Phys. Rev. B **83**, 214501 (2011).

[38]C. G. Shull and F. A. Wedgwood, Phys. Rev. Lett. **16**, 513 (1966).

[39]C. Stassis, J. Arthur, C. F. Majkrzak, J. D. Axe, B. Batlogg, J. Remeika, Z. Fisk, J. L. Smith, and A. S. Edelstein, Phys. Rev. B **34**, 4382 (1986).

[40]J. Boucherle, J. Henry, R. J. Papoular, J. Rossat-Mignod, J. Schweizer, F. Tasset, and G. Uimin, Physica B **192**, 25 (1993).

[41]J. A. Duffy, S. M. Hayden, Y. Maeno, Z. Mao, J. Kulda, and G. J. McIntyre, Phys. Rev. Lett. **85**, 5412 (2000).

[42]K. Yosida, Phys. Rev. **110**, 769 (1958).

[43]A. M. Clogston, A. C. Gossard, V. Jaccarino, and Y. Yafet, Phys. Rev. Lett. **9**, 262 (1962).

[44]H.-J. Grafe, D. Paar, G. Lang, N. J. Curro, G. Behr, J. Werner, J. Hamann-Borrero, C. Hess, N. Leps, R. Klingeler, and B. Büchner, Phys. Rev. Lett. **101**, 047003 (2008).

[45]S. Graser, T. A. Maier, P. J. Hirschfeld, and D. J. Scalapino, New J. Phys. **11**, 025016 (2009).

[46]In this section, we choose the unit cell origin to be at an Fe site. With this convention, $M(\mathbf{G} = 002)$ is positive and corresponds to a positive susceptibility.

[47]G. E. Volovik, JETP Lett. **58**, 469 (1993).

[48]C. Caroli, P. G. D. Gennes, and J. Matricon, Phys. Lett. **9**, 307 (1964).

[49]Y. Nakai, T. Iye, S. Kitagawa, K. Ishida, S. Kasahara, T. Shibauchi, Y. Matsuda, and T. Terashima, Phys. Rev. B **81**, 020503 (2010).

[50]Ref. 11 reported that the residual specific heat can be reduced by annealing.

[51]J. Guo, S. Jin, G. Wang, S. Wang, K. Zhu, T. Zhou, M. He, and X. Chen, Phys. Rev. B **82**, 180520 (2010).

[52]I. Mazin, Phys. **4**, 26 (2011).